A hybrid modal decomposition approach for higher-order modes in circular ducts

J.L. Horner & Y.Hu

Department of Aeronautical & Automotive Engineering

Loughborough University, Loughborough, LE11 3TU, United Kingdom

Corresponding author. Tel.: +44(1509) 227204

E-mail address: j.l.horner@lboro.ac.uk

Abstract

Before it is possible to determine the effect over a wide frequency range of different aperture devices on the sound field in a duct, the contribution from the individual higher-order modes must be established. Two approaches to decompose the sound field may be taken which are either to use a large number of microphone locations to reconstruct the sound field, or to use a hybrid method involving a reduced set of microphone locations and a model of the sound field in the system. Modelling the higher-order modes in a duct is itself a numerically intensive procedure if fully coupled calculations are required. It is possible to simplify the process for modelling the sound field by using uncoupled calculations for the higher order modes. Results are presented for such a hybrid approach, combining a limited number of microphone locations with an uncoupled model, to establish the sound field in a circular duct. Both point source and plane wave sources are considered and direct measurement of the sound field is compared to the reconstructed field for a normalised wave number range up to 7. Results show acceptable agreement between the hybrid approach and direct measurement with the greatest errors occurring around cut-on of the axially anti-symmetric modes. Thus, it is demonstrated that a hybrid approach may be applied to ducts with simple sources and that the approach can be used to deconstruct the in-duct sound field into the individual higher-order mode contributions

1 Introduction

Many engineering products contain ducts of constant cross-section that conduct sound and may require the installation of aperture devices, such as orifice plates. Research on the acoustic performance of such devices has mainly focused on the specific application and no generic approach has been taken. Before a generic approach for the analysis of aperture devices can be developed, methods for simply establishing the individual modal contributions to the overall in-duct field must be developed.

In order to study the acoustic properties over a wide frequency range, consideration must be given to the propagation of the higher-order modes in the system. To fully understand the effects of any device, once the first higher-order mode cuts-on in the duct, it is necessary to decompose the in-duct field into the different single higher-order modal amplitudes. There are two possible approaches to decompose measurements of the in-duct field into the individual higher-order mode contributions. These are either a wholly experimental decomposition approach using a large number of microphone locations or a hybrid approach using a limited number of microphone positions and estimates for the modal reflection coefficients taken from theoretical models. However, the calculation of the reflection coefficients can itself be a numerically intensive activity, if fully coupled calculations of the possible higher-order modes are used. Thus, any hybrid decomposition approach that uses fully coupled calculations for the higher-order modes is impractical to use due to the time required to estimate the field. This can be reduced by using approximate values for the modal reflection coefficients obtained by ignoring the cross coupling terms between modes in the calculation and, thus, making a hybrid approach applicable to use.

The theoretical approaches, which govern the wave propagation in circular ducts, have been discussed in detail and are fully presented in, for example, Refs. [1] and [2]. One model to calculate the generalized radiation impedances of all modes in circular ducts, which was terminated with an infinite baffle, was given in Ref. [3]. The equation for the generalized radiation impedance was reduced to a single infinite integral which was a function of the mode radiation directivity factors. Then, an infinite matrix equation was derived to relate the generalized mode reflection

coefficients to the radiation impedances. By knowing the complex reflection coefficients, it was possible to relate the reflected amplitudes with the incident amplitudes and then to decompose the in-duct field into different higher-order modes. This analysis was extended in Ref. [4] to obtain approximate expressions for the radiation impedances for practical engineering applications.

Two-microphone methods such as those introduced in Refs. [5] and [6] have been widely studied for the measurement of acoustic properties in ducts such as reflection coefficients. In Ref. [5], the author discussed the possible errors introduced by this method. In order to minimize the errors, it was suggested that the overall length of the duct be kept small, in practice, the length should be between five and ten times the duct diameter; the source end of the duct should be as non-reflective as possible; microphones should be high coherence and the separation between the microphone pairs should be small. Discussions of the first helical mode's contribution to the plane wave were made in Ref. [6]. In this, the authors placed two receiver microphones in the same plane with the speaker. This arrangement allowed a better measurement of the plane wave up to the cut-on frequency of the second higher-order mode and, hence, was able to isolate the first higher-order mode.

A multiple-microphones method [7] was proposed for the measurement of the acoustic properties in ducts and some guidelines for the selection of proper microphone positions were also provided. Although the two-microphones method was accepted as the standard method for the measurement of the in-duct acoustic properties, results on using the least square method with multiple measurement points have been reported for enhancing the frequency response of the two-microphones method. By increasing the number of the microphones, one could improve the measurement accuracy and increase the effective frequency range. A direct modal decomposition of the in-duct field was carried out in Ref. [8]. The author focused on the separation of the radial modes and made a comparison of three methods. Through the comparison, it was found that the least squares method was the best one, because the matrix method was prone to instability and the integration method had a relatively high noise floor. According to the study, it was possible to separate the in-duct field into different modes even when there were a larger number of higher-order modes propagating in circular ducts. The number of the measuring points should be twice the product of the maximum number of propagating circumferential modes and the

maximum number of propagating radial modes for any circumferential order. But in practice, many more points were needed to average out the measurements errors.

The instantaneous mode separation method, which could separate the broadband noise propagating inside circular ducts into different higher-order modes, was developed in Ref. [9]. In this method, $2n$ pressure transducers spaced evenly around the circumference of the duct were used to separate the (n-1) order of circumferential modes. This method had the advantage of not needing circumferential traversing of the microphone array, and so the circumferential separation did not involve matrix solutions, which were sensitive to small measurement inaccuracies. However, the approach also had a limitation, which was that it could only separate the axially symmetric circumferential modes. Another in-duct modal decomposition technique, which was based on the transfer function measurements between microphone pairs, was described in Ref. [10]. The rationale for using this method was that the transfer functions had two significant advantages. Firstly, transfer functions were independent of the signal type in the ducts and, secondly, transfer functions were in many cases less sensitive to bias and random errors than other spectral quantities. By using this approach, the author could separate the in-duct field into incident and reflected waves from measurements at two axial positions. Again, this method was also only valid for the separation of the circumferential modes.

From the discussion above, it may be seen that the experimental decomposition of higher-order modes is complex and that many methods are only practical for the axially symmetric circumferential modes. So it is important to establish other approaches for the modal decomposition in circular ducts. As discussed by Åbom [10], the experimental decomposition approaches can be divided into two main types: direct approaches and correlation approaches. The basis for the direct approaches is simultaneous measurements of an acoustic field quantity, such as acoustic pressure, at a number of measurement positions. For the correlation approaches, the basis is the space-time correlation of an acoustic field quantity between several pairs of measurement points. These two approaches basically perform the modal decomposition either by a two-dimensional spatial Fourier Transform over the duct cross-section or by the solution of a linear equation system. These equations can then be solved using a matrix approach. However, use of the wholly experimental decomposition method can lead to large errors in the decomposed modal contributions. The sources for the large errors usually are the

result of the measurement positions not being fully independent of each other, which makes the system matrix badly conditioned. In addition, the system matrix is sensitive to small measurement errors, which can cause a large error in the final results.

Hence the proposed hybrid decomposition method reported in this paper. This method uses a limited number of measurement locations in the duct and then applies the estimates from uncoupled calculations of the fields to obtain the parameters for the higher-order modes rather than reconstruct the whole field from many direct measurements. If separation of the higher-order modes can be achieved via this method, then it would be easier to study the modal properties of any devices. The validity of the approach can be tested by comparing the reconstructed field from the hybrid method with direct measurements of the in-duct field.

In the following analysis two different types of the sound source, a plane wave source and a point source, will be considered. These were selected to allow consideration of concentric and eccentric located sources of the same type. Analytical approaches combine the different descriptions of the sound sources with that of a flanged duct open end and, hence, the estimates for the acoustic properties can be obtained. The plane wave source is an extension of the point source analysis, as the plane wave analysis will consider two acoustic fields, the source field and the main duct field. A rigid aperture plate containing a small office physically separates the fields. The plane wave is developed in the source field between the source and the aperture plate and then excites the main duct field between the aperture plate and the flanged open end. Thus, the plane wave source also demonstrates the application of the approach for a duct with a simple aperture device. For the experimental work, a circular cross-section duct with a flanged end was used as the main duct. The measurements were divided into two categories, these were reference measurements, which were used for the hybrid decomposition approach and direct measurements, which were used for the comparison with the reconstructed field obtained from the hybrid approach. Results are presented for both point source and plane wave excitation.

2 In-duct acoustic field

For the open-ended boundary of a circular duct, if the length of the duct is infinite and there are no other obstacles within it, the in-duct field only contains

incident propagating waves. In this situation, every mode is independent of each other and there is no energy transfer between different higher-order modes. Hence, no cross coupling effects appear in the equation below:

$$p_A = j\rho\omega \sum_{m=0}^{\infty} \sum_{n=1}^{\infty} J_m(k_{r,m,n} r)(A^{+}_{m,n} e^{-jm\varphi} + A^{-}_{m,n} e^{jm\varphi}) e^{j\omega t} e^{-jk_{z,m,n} z} . \quad (1)$$

Where P_A is pressure, ρ is density, ω is frequency, k is the wave number, and $A^{+}_{m,n}$ and $A^{-}_{m,n}$ are the incident wave amplitudes. The co-ordinates of the point of interest are given by z, r and φ.

However, if the length of duct is finite or there are discontinuities in the duct, then at these points, there will be a reflection of the incident wave and the in-duct field in this situation is composed of both incident and reflected waves. So for the reflected field, the reflected waves can be written in the form:

$$p_B = j\rho\omega \sum_{m=0}^{\infty} \sum_{n=1}^{\infty} J_m(k_{r,m,n} r)(B^{+}_{m,n} e^{-jm\phi} + B^{-}_{m,n} e^{jm\phi}) e^{j\omega t} e^{jk_{z,m,n} z} . \quad (2)$$

Where $B^{+}_{m,n}$ and $B^{-}_{m,n}$ represent the possible reflected wave amplitudes.

There will be some energy transfer from the other higher-order modes to this mode resulting from the discontinuities of the duct and vice-versa some energy transfer from this mode to other higher-order modes. Expressing these reflected wave amplitudes in the form of the complex reflection coefficients [3] then gives

$$B_{mn} = \sum_{L=1}^{\infty} R_{mnL} A_{mL} . \quad (3)$$

This equation represents a fully coupled situation and allows for possible energy transfer between modes. For an uncoupled equation, the assumption is made that the cross-coupling effects between higher-order modes are so weak that the energy transfer between different modes is small and can be neglected. So the amplitude of each reflected mode B_{mn} consists only of the reflection of the corresponding incident mode, A_{mn}, which can be written as

$$B_{mn} = R_{mnn} A_{mn} \ . \tag{4}$$

However, for the fully coupled calculation, according to Eq. (3), the amplitude of B_{mn} should include the contributions of all other higher-order modes with the same subscript value *m*. So the uncoupled formulation ignores contributions from all other modes, both propagating and cut-off. Also the uncoupled calculation need only be performed for the modes of interest rather than all possible modes in the frequency range of interest. Thus, obtaining estimates for the uncoupled modal reflection coefficients requires significantly less computational effort than a fully coupled calculation [11].

To determine the complex reflection coefficient R_{mnl}, the model proposed by Zorumski [3] for a circular duct terminated with an infinite, rigid baffle was used. It was assumed that the duct wall was hard and the specific admittance of the duct wall was set to zero. The impedance of the duct was calculated for a set of higher-order modes and then used to determine the reflection coefficients for the modes. Following the analysis presented in Ref. [3], the generalized impedance of the duct is given by

$$Z_{mnL} = j\int_0^{\infty} \tau(\tau^2 - 1)^{-1/2} D_{mn}(\tau) D_{mL}(\tau) d\tau \ . \tag{5}$$

Where

$$D_{mn}(\tau) = k^2 \int_0^R r_0 J_m(\tau k r_0) J_m(k_{r,m,n} r_0) / N_{mn} dr_0 \ .$$

The normalizing factor N_{mn} is given by Ref. [12] as

$$N_{mn} = kR\left\{0.5\left[1 - (\frac{m}{k_{r,m,n}R})^2\right] J_m(k_{r,m,n}R)^2 + J_m^{'2}(k_{r,m,n}R)\right\}^{1/2}, \tag{6}$$

and in the above equations R is the internal radius of the duct and r_0 is the co-ordinate of the point of interest.

Thus, it may be shown that the generalized reflection coefficients may be obtained from the following infinite matrix

$$[R_{mnL}] = [[Z_{mnL}][\frac{k_{z,m,L}}{k}] + [I]]^{-1}[[Z_{mnL}][\frac{k_{z,m,L}}{k}] - [I]], \tag{7}$$

in which $[I]$ is the unit matrix (identity matrix).

As discussed in Chapter IV of Ref. [13] by S. N. Rschevkin, for a point source backed by a hard baffle, the particle velocity is related to acoustic pressure by

$$v_s = \frac{p(kl - j)}{\rho ckl}, \tag{8}$$

in which, l is the distance from the point source. If the radius of the source is very small, then the value of Helmholtz number kl is nearly equal to zero. Thus compared with unity, it can be ignored, so the above equation can be expressed as

$$v_s \approx \frac{-jp}{\rho ckl} = \frac{Q}{2\pi l^2} e^{j(\omega t - kl)}, \tag{9}$$

in which Q is the source strength. Mode matching techniques may then be applied to establish an analytical model of the flanged duct excited by a point source, described using the above equation, and used to determine the amplitudes of the in-duct waves [14,15]. It is possible to develop sufficient equations to solve for the wave amplitudes in the duct. It should be noted that the position of the source has to be known as the co-ordinates of the source are required as inputs to the model.

The plane wave source is an extension of the point source model where the source is modeled as a point source in a small duct connected to the main duct via a rigid aperture plate. The source duct is of such a small radius that only the plane wave propagates in the source duct. Then the plane wave excites the field in the main duct. Mode matching was again used to model the interface between the source duct and the main duct. As the plane wave model contained both the source field and the

in-duct field, the number of independent equations required to estimate the amplitudes was greater than the point source model. For example, if m = +/-4 and n = 4, 144 equations were required to determine the unknown wave amplitudes. By modeling the plane wave source in this way, this also provided a model of a duct system containing an aperture device. Results from the mode matching models were calculated using both fully coupled and uncoupled calculations to compare the two estimates.

3 Measurement procedure for hybrid approach

All measurements were made on a circular mild steel duct of length 3 m and internal radius 0.15 m that at one end was terminated with a large rigid baffle.. The duct satisfied the length to diameter condition [5] that in order to minimize errors the length of the duct should be between 5 to 10 times the duct diameter. At the other end of the duct a source could be connected, via a source duct, to the main duct. Two different types of source were used in the experimental investigations, which were a point source and a plane wave source. The whole system was placed in the middle of an anechoic chamber of volume 362 m^3 and the lower frequency limit for the chamber was 100 Hz. All measurements were made with half-inch microphones, mounted in the wall of the main duct.

For the point source excitation, a 0.9 m long circular duct of internal radius 0.0075 m was used as the source duct. One end of the source duct was connected to an enclosed loudspeaker. At the other end, it was connected to a rigid plate containing a circular hole of the same radius. The whole system was then installed at the end of the main duct, so that the rigid plate was the interface between the source duct and the main duct, as shown in Fig. 1. It was considered that the smaller the source duct radius then the better the approximation to a true point source. In this investigation, the ratio of the two duct radii was 5%. In the frequency range used, 10-2600 Hz, the value of the Helmholtz number in the source duct was $k * R_p \leq 0.36$, which was far less than the first higher-order mode $(\pm 1, 1)$ cut on value of 1.84. In the frequency domain, the $(\pm 1, 1)$ mode cut on in the main duct at 640 Hz.

Rigid plates with the point source located at different radial distances from the centre were used. Fig. 1 shows the experimental set-up and the locations of the

microphones. Using the baffled end of the duct as the origin of the coordinate system, two different locations z = - 0.54 m and z = - 0.18 m were considered. At each location, around the circumference of the duct, there were six equally positioned measurement points, as shown in Fig. 1. Each measuring point was blocked when not in use.. Data recorded at these locations were considered to represent a direct measurement of the acoustic field and used as a comparison to the results obtained from the hybrid decomposition approach. Other microphones were located at (0.15 m, 0 degs., -2.33 m) and (0.15 m, 275 degs., -1.5 m) and were used for the reference measurements for the hybrid approach. This meant reference measurement 1 was located at -78%L and reference measurement 2 was located at -50%L, whereas the direct measurements were located at either -18%L or -6%L. Thus the reference measurement positions were located away from the source and the baffled end to reduce the contribution from the evanescent modes. The reasons for using two reference measurements, rather than one, was firstly that by utilising different circumferential angles, it is possible to capture information for the spiraling higher-order modes. Also by utilising different z-axis values, it was possible to separate incident waves and reflected waves more accurately. Finally, by considering two reference positions, it reduced the random measurement errors introduced by using only one reference point.

As stated above, the frequency range used for the measurements was 10-2600 Hz, which equated to a normalised wave number, kR, range up to 7. In this range nine higher modes were cut-on in the duct when the point source was placed off-centre. These consisted of a combination of symmetric and anti-symmetric modes. If the point source was positioned on the centre-line of the duct, only the axially symmetric, (0,n), modes were excited. As the values of the wave amplitudes were required for comparison with the direct measurements, the amplitude of the volume velocity, U, of the source was determined first from the two reference measurements.

The measurements were divided reference measurements and direct measurements. The direct measurement results were used to compare with the results obtained by the hybrid modal decomposition approach. The reference measurement results were used in the hybrid approach to estimate the amplitudes of the acoustic properties in the duct. The procedure of the application of the reference measurements used in the hybrid decomposition approach was as follows. Firstly, a matrix solution for the duct termination reflection coefficient was set up using uncoupled equations

for the cut-on modes of interest. Then, in the matrix the amplitude of the volume velocity U was set equal to unity and the coordinates of reference position 1 were substituted into the matrix to obtain the relative amplitudes of A_{mn} and B_{mn}. By substituting these relative amplitudes and the coordinates of the reference point into Eq. (1), it was possible to get the estimated relative acoustic pressure at the reference point. By comparing this relative acoustic pressure with the actual pressure, the reference measurement, it was possible to obtain the ratio between the actual pressure and relative acoustic pressure (P_{act} / P_{comp}). This ratio was then assumed be equal to the actual amplitude of the volume velocity U. The procedure was then repeated for reference measurement position 2 to obtain another value of the amplitude of the volume velocity U. The average of these two volume velocity estimates was taken as the amplitude of the volume velocity and substituted into the matrix, thus, allowing the values of the amplitudes A_{mn} and B_{mn} to be estimated. Finally, these amplitudes and the coordinates of any measurement point were substituted into the acoustic pressure Eq. (1), to obtain the estimated acoustic pressures at any point in the duct. After determining the actual amplitudes of different modes, the in-duct field was then decomposed into the different modal contributions

The configuration of the plane wave sound source is shown in Fig. 2, and for this source a duct with a radius of 0.024 m was used as the sound source. For the frequency range used in the investigation, the Helmholtz number in the plane wave source duct was less than kR = 1.15 at the highest frequency. The length of source duct used for the plane wave source was 0.94 m. Thus, the source duct for the plane wave source was approximately the same length as that used for the point source but had a greater radius, by a factor of 3.2 than the source duct used for the point source. As the value of Helmholtz number in the plane wave source duct at the highest test frequency was less than the first higher-order mode cut-on value of kR = 1.84, that meant that only the plane wave could propagate in the source duct. So this type of source was considered as an estimate for a plane wave source. However, it should be noted that at the interface between the source and the main duct or even at a very small distance from the interface, there would be many cut-off higher-order modes present. Contributions from these cut-off modes were not included in the uncoupled calculations used for the estimates for the fields.

The procedure to obtain the estimates for the acoustic pressure in the main duct for the plane wave source was the same as for the point source. Originally the two reference measurements were made in the plane wave source duct, rather than the main duct. However, due the small radius of the plane wave source duct, it was not possible to obtain good measurement results as it was more difficult to mount the microphones flush to the wall of the source duct. Also it was considered that microphones needed to be located in the main duct region to capture the higher-order modes information more accurately. As with the point source, a matrix solution for the system, including both the source duct and the main duct, was constructed using uncoupled analysis. The same two reference measurement positions were chosen in the main duct as for the point source. In the plane wave case the reference measurements were used to estimate the amplitude of the incident wave in the source duct. As with the point source, testing was undertaken with the plane wave source located at different radial distances from the centre of the duct so as to investigate the effect of source position on the results.

4 Results for point source excitation

Before considering the difference between the estimates from the hybrid approach for the position -18%L with the direct measurement at that point, a comparison was made between using the coupled or the uncoupled calculations of reflection coefficients to determine the amplitudes of a single higher-order mode. Take the $(\pm 1,1)$ modes, for example, which are the first higher-order modes cut-on in the duct and are axially anti-symmetric. In Fig. 3, three comparisons are plotted to illustrate the different modal amplitudes. Fig. 3a shows the comparison between the amplitude of incident mode A_{11}^{+} and reflected mode B_{11}^{+}; Fig. 3b shows the comparison between the amplitude of A_{11}^{+} and A_{11}^{-} and Fig. 3c shows the comparison between the amplitude of A_{11}^{+} obtained from the coupled prediction and from the uncoupled prediction. Results are presented in the normalised wave number format so the $(\pm 1,1)$ mode would cut-on at a value of 1.84. From Fig. 3b, it may be observed that the amplitude of A_{11}^{+} equals to amplitude of A_{11}^{-}. From this figure, it can also be seen that the amplitudes of those higher-order modes cut-on at the respective cut-on wave

numbers and then decay very quickly with increasing wave number. The coupling effects at the flanged open end of the duct can be neglected, because the amplitudes obtained from the coupled prediction are equal to those obtained from the uncoupled prediction, as shown in Fig. 3a. Similar comparisons between uncoupled and coupled predictions were obtained for other modes.

Based on the modal amplitudes obtained from both the uncoupled and coupled equations, it was possible to reconstruct the acoustic pressure at any point in the main duct using the data measured at the two reference locations, as outlined in the previous section. A point located at z = -0.54 m is taken as an example of the reconstructed acoustic field, using the hybrid approach. This point was -18%L where as the two reference locations were -50%L and -78%L. The estimated pressure using coupled analysis, the estimated pressure using uncoupled analysis and the directly measured pressure at this point are shown in Fig. 4. The sound source was located at δ = 0.0 m (0%R), the concentric situation, so that only axially symmetric, (0,n) modes were cut-on in the duct. Then at δ = 0.06 m (40%R), the eccentric situation, to ensure that both axially symmetric and axially anti-symmetric modes were cut-on in the duct. In order to show the comparison between results more clearly, in Fig. 5 the linear frequency data is transferred to 1/6 octave band data. Compared with 1/3 octave band representation, 1/6 octave band can give more detailed information for the higher normalised wave number range. Fig. 5c shows the percentage error between the estimated pressure established using uncoupled predictions and the direct measurement of the pressure. Similar results were obtained for the other location, -6%L, in the duct. With the exception of very low values of kR, the errors between the partially coupled prediction and the direct measurement mainly fall into the range $\pm$10% of the direct measurement (or even smaller), which were considered to be acceptable considering the significant reduction in computational analysis time by using the hybrid approach. The large error around approximately kR = 0.3, was discounted as this was at the lower limit of the useable frequency range of the anechoic chamber. The largest errors in the higher mode region occurred around the cut-on wave numbers for some of the anti-symmetric modes. For example, in the eccentric source situation, the (2,1) mode cuts on at kR = 3.05 and the largest error occurred in the region around kR = 2.8 to 3.4. Also the (5,1) mode cut-on at kR = 6.41 and the (2,2) mode at kR = 6.71. As the uncoupled analysis ignored the

contributions from cut-off modes, it was expected that the largest errors using the hybrid approach would occur around cut-off when the evanescent contribution from a mode was growing as the mode changed from cut-off to cut-on.

From Fig. 5 the effects of spiralling anti-symmetric higher-order modes on the estimates from the hybrid approach could be observed, In order to establish whether or not the hybrid approach could successfully reconstruct the spiralling higher-order modes, different points around the circumference of the main duct were investigated. As shown in Fig. 1, in the main duct, there were two sets of circumferential measurement points, each with six equally distributed measurement positions. In the following two figures, Figs. 6 and 7, position 1 refers to point 1 on Fig. 1, position 2 to point 3 and position 3 to point 5. So each position is separated by 120 degrees. Fig. 6 shows the pressures when the source duct is concentric to the main duct ($\delta = 0m$) and Fig. 7 shows the pressures when the source duct is eccentric to the main duct ($\delta = 0.06m(40\%R)$). For the concentric situation, shown in Fig 6, there was very little difference between the estimates or predictions for the three positions, but for direct measurements, there was a small difference between these three positions, which may have been caused by measurement errors or by positioning errors in the location of the source duct. If the source duct was not perfectly concentric to the main duct, then the anti-symmetric modes would have propagated in the main duct. However, the measurements for the three positions were quite similar as would be expected if the in-duct field were dominated by the symmetric (0,*n*) modes. So the errors between the predicted and direct measurement were similar and, therefore, considered acceptable,

For the eccentric situation, shown in Fig. 7, other higher-order modes were cut-on and propagated in the main duct. Both predictions and direct measurements for these three positions were very different due to the spiralling higher-order modes. By comparing the errors for the three positions, it was observed that the errors for all these three positions were largest around the normalized wave number range of kR = 3, which is just around the $(\pm 2,1)$ modes cut-on wave number, similar to Fig. 5. The errors were all different for the three positions, which implied that prediction around the circumference of the duct for the eccentric source situation was dependent on the circumferential angle and the wave number or frequency range.

For both the concentric and the eccentric source situation, compared with other parts of the wave number range, the low normalized wave number range

prediction had the largest errors. This had been observed in other results and was discounted as it was below the lower frequency limit of the anechoic chamber. It was observed that for both the concentric and the eccentric source locations the errors between the predictions and the direct measurements fell mainly into the range $\pm 10\%$ of the direct measurements, which is considered acceptable for the estimates.

5 Results for plane wave source excitation

Fig. 8 shows results for the plane wave source, with the direct measurement made at the same location as the point source. As before two source locations are considered which are the concentric and the eccentric ($\delta = 0.06m(40\% R_0)$) locations. Fig. 8a shows the coupled and uncoupled estimated pressures and directly measured pressures for the concentric source duct situation. Fig. 8b shows the coupled, and uncoupled estimated pressures and directly measured pressures for the source duct located at the eccentric situation. From this figure it may be seen that there is very little difference between the coupled and the uncoupled estimates. Another eccentric source location, where the source was located at 0.09 m (60%R) was also investigated. Fig. 9 shows the 1/6 octave band representation of the three source locations and the error associated with each. It can be seen in Fig. 9 that apart from the low normalized wave number range, the errors between the estimates and the direct measurements mainly fall into the range of $\pm 5\%$ of the direct measurements, especially for the concentric situation. Similar size errors were found for the two eccentric situations with the errors increasing with the increased eccentricity of the source. In the concentric situation, the errors were smaller because only the axially symmetric higher-order modes were dominant in the main duct. For the eccentric situations, axially anti-symmetric higher-order modes were dominant in the main duct and there are many more modes present. As with the point source, the greatest errors occurred around the cut-on wave number for a mode. In Fig. 9, it may be observed that the first noticeable error occurs around the cut-on wave number for the (1,1) mode, that cuts on at kR = 1.84. It is not surprising that the errors increased with increased eccentricity of the source as the anti-symmetric modes would be stronger the further the source was located from the duct axis.

In the previous section comparisons were made between predictions and measurements for different circumferential positions on the duct. This analysis was repeated to test the accuracy of the predictions for the same circumferential positions for the plane wave source. Fig. 10 shows the situation when the plane wave source duct was concentric to the main duct and Fig. 11 shows the situation when the plane wave source duct was eccentric to the main duct ($\delta = 0.06m(40\% R_0)$). In Figs. 10 and 11: a) shows the direct measurements at the three positions on the circumference; b) shows the estimate or prediction for the three positions; and c) shows the errors between predictions and direct measurements for the three positions. As with the point source, for the concentric situation, Fig. 10, there was no difference for the predictions for the three positions, but in the direct measurements, there was a small difference between these three positions. The errors between the predictions and the direct measurements were similar and, therefore, considered acceptable. For the eccentric situation, other higher-order modes were cut-on and propagate along the duct, as may be observed in Fig. 11. Both predictions and direct measurements for the three positions were different, which is caused by the spiralling higher-order modes. By comparing the errors for the three positions, it was observed that these errors are different at different parts of the normalized wave number range. For example, before the $(\pm 1,1)$ modes cut-on, the errors for these three positions are nearly the same and after the $(\pm 1,1)$ modes cut-on at kR = 1.84, the errors for these three positions were different. As with the point source, this implied that the prediction around the circumference for the eccentric source situation was dependent upon the circumferential angle and the wave number or frequency range. The errors for the three positions were mainly less than 10% of the direct measurements, apart from the low normalized wave number range.

6 Conclusion and discussion

A practical approach for the decomposition of the in-duct acoustic field has been established that combines the theoretical and experimental decomposition approaches together. Unlike other approaches, it makes the decomposition of the in-duct field for circular ducts less experimentally intensive as only two measurement

locations are required. From the results presented, it can be seen that the proposed hybrid decomposition approach was successfully applied to a duct without any apertures device, i.e. the point source case; and a duct containing a simple single orifice plate, i.e. the plane wave source case. The results for the plane wave source indicate that the approach could be successfully extended to ducts containing simple aperture devices, as for this source two acoustic fields had to estimated. This is the same as estimating the fields before and after an aperture device in a duct. Obviously, the limitation on the hybrid approach is the requirement to develop an approximate analytical model of any aperture device by using mode-matching techniques. Also the approach requires the co-ordinates and type of the source to be known. It should be noted that if the source is incorrectly assumed to be concentric then errors will occur as only the (0,n) modes will be included in the uncoupled model and hence modes will be missing from the estimate. For the plane wave source, which involved a single orifice plate with a single circular opening, the analytical model required the solution of 144 equations to decompose the field. As the aperture device become more complex, the number of equations would significantly increase along with the inherent errors in solving large sparsely populated matrices. It should also be noted that the differences between the estimates from the hybrid model and the direct measurements were generally less for the plane wave source. In the experiments, the actual sound sources could only approximate the desired source type. It is likely that the plane wave source was a better approximation to the desired one than the point source. However, the total errors inherent in the hybrid approach, which include errors caused by the model description, the neglecting of the contribution from the cut-off higher-order modes in the model and any measurement errors in the procedure are considered acceptable. It may be concluded that within acceptable error bands that the hybrid approach can be used to deconstruct the in-duct field into the individual higher-order modal contributions. The greatest errors occur in the frequency region just before a mode is cut-on as the uncoupled model does not include evanescent contributions. To reduce the errors further, these contributions would need to be accounted for in the uncoupled model

7 References

1. Morse PM, Ingard KU. Theoretical acoustics. Princeton University Press; 1986.
2. Munjal ML. Acoustics of ducts and mufflers with application to exhaust and ventilation system design. John Wiley & Son; 1987.
3. Zorumski WE. Generalized radiation impedances and reflection coefficients of circular and annular ducts. J Acoust Soc Am 1973;54(6):1667-1673.
4. Silva F, Guillemain P, Kergomard J, Mallaroni B, Norris AN, Approximation formulae for the acoustic radiation impedance of a cylindrical pipe. J Sound Vibr 2009;322:255-263.
5. Bodén H, Åbom M. Influence of errors on the two-microphone methods for measuring acoustic properties in ducts. J Acoust Soc A 1986;79(2):541-548.
6. Dalmont J, Bruneau A. Acoustic impedance measurement: plane-wave and first helical mode contributions. J Acoust Soc Am 1992;91(5):3026-3033.
7. Jang S, Ih J. On the multiple microphone method for measuring in-duct acoustic properties in the presence of mean flow. J Acoust Soc Am 1998;103(3):1520-1526.
8. Moore CJ. Measurement of radial and circumferential modes in annular and circular fan ducts. J Sound Vibr 1979;62:235-256.
9. Kerschen EJ, Johnston JP. A modal separation measurement technique for broadband noise propagating inside circular ducts. J Sound Vibr 1981;76:499-515.
10. Åbom M. Modal decomposition in ducts based on transfer function measurements between microphone pairs. J Sound Vibr 1989;135:95-114.
11. Horner JL, Lyons R, Petersson BAT. Approximations for modal coupling in scattered fields from orifices. J Acoust Soc Am 2000;108(2):488-493.
12. Watson GN. A treatise on the theory of Bessel functions. Cambridge University Press; 1958.
13. Rschevkin SN. A course of lectures on the theory of sound. Pergamon Press; 1963.
14. Muehleisen RT, Swanson DC. Modal coupling in acoustic waveguides: planner discontinuities. Appl Acoust 2002;63:1375-1392.
15. Hu Y. A generic approach for the study of higher-order mode propagation in circular ducts with simple aperture devices. Ph.D. Thesis, Loughborough University; 2007.

List of Figure Captions

Fig. 1. Experimental arrangement for the point source measurement.

Fig. 2. Configuration of the plane wave source in the circular duct.

Fig. 3. Comparison of the amplitudes of the $(\pm 1,1)$ mode with point source excitation.

Fig. 4. Comparison between the coupled predictions and the direct measurements for point source excitation: *a*) source concentric ($\delta = 0m$); *b*) source eccentric ($\delta = 0.06m(40\%R)$)).

Fig. 5. Comparison between the coupled predictions and the direct measurements for point source excitation: *a*) source concentric ($\delta = 0m$); *b*) source eccentric ($\delta = 0.06m(40\%R)$); *c*) percentage errors.

Fig. 6. Comparison of the errors around the circumference of the main duct for a concentric point source: *a*) direct measurements; *b*) predicted results; *c*) percentage errors.

Fig. 7. Comparison of the errors around the circumference of the main duct for an eccentric point source: *a*) direct measurements; *b*) predicted results; *c*) percentage errors.

Fig. 8. Comparison of the coupled and uncoupled predictions with direct measurements for the plane wave source: *a*) source concentric ($\delta = 0m$); *b*) source eccentric ($\delta = 0.06m(40\%R)$)).

Fig. 9. Comparison of the errors for the concentric and eccentric plane wave source: *a*) source concentric; *b*) source eccentric $\delta = 0.06m(40\%R_0)$; *c*) source eccentric $\delta = 0.09m(60\%R_0)$; *d*) percentage errors

Fig. 10. Comparison of the errors around the circumference of the main duct for a concentric plane wave source: *a*) direct measurements; *b*) predicted results; *c*) percentage errors.

Fig .11. Comparison of the errors around the circumference of the main duct for an eccentric plane wave source: *a*) direct measurements; *b*) predicted results; *c*) percentage errors.

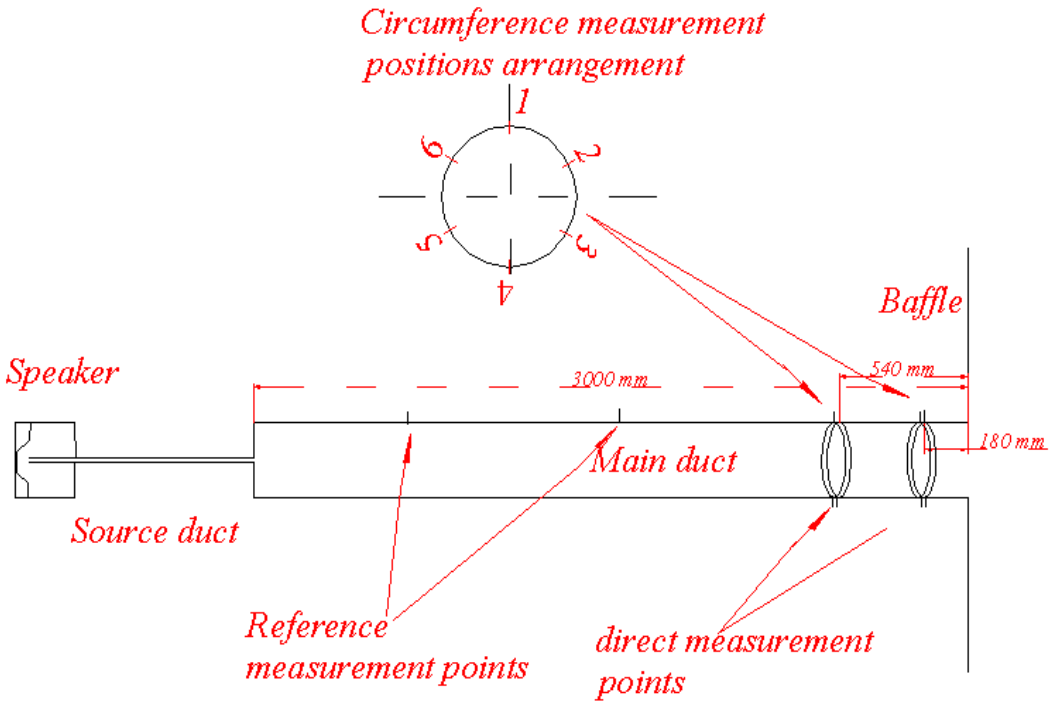

Fig. 1. Experimental arrangement for the point source measurement.

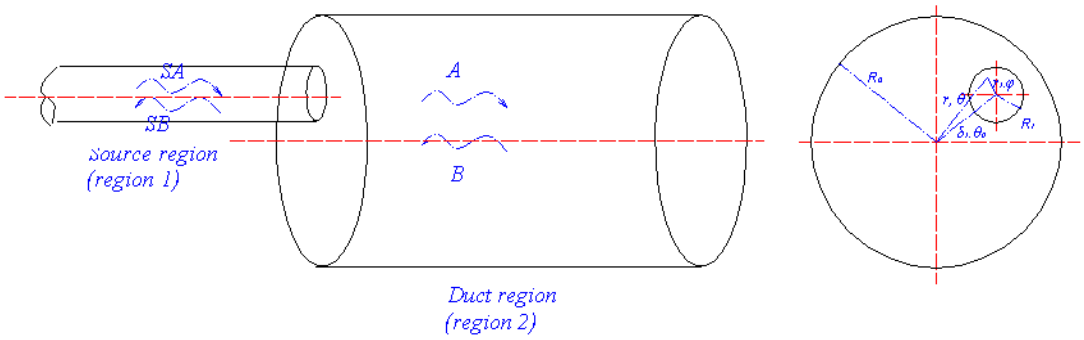

Fig. 2. Configuration of the plane wave source in the circular duct.

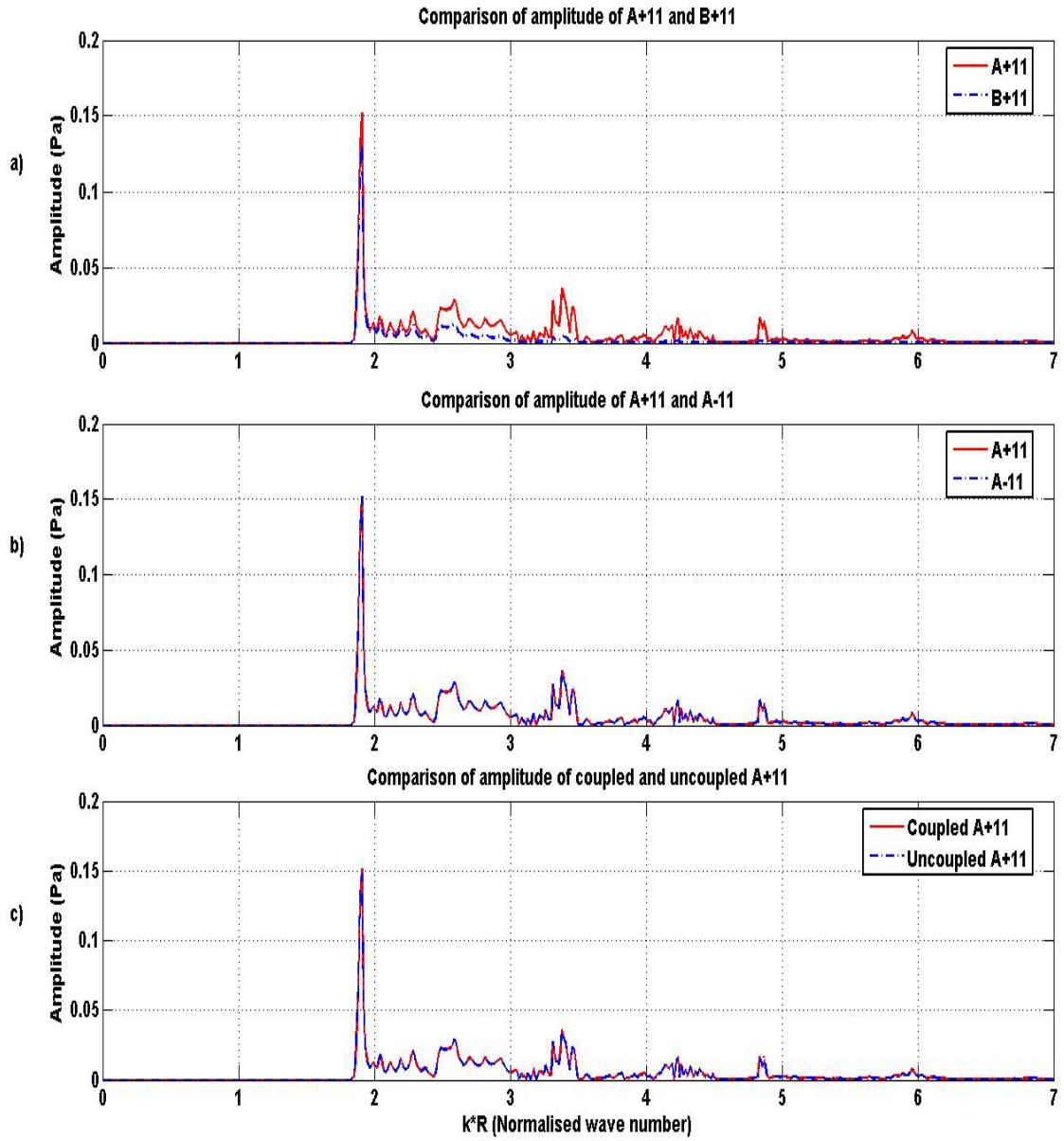

Fig. 3. Comparison of the amplitudes of the $(\pm 1,1)$ mode with point source excitation.

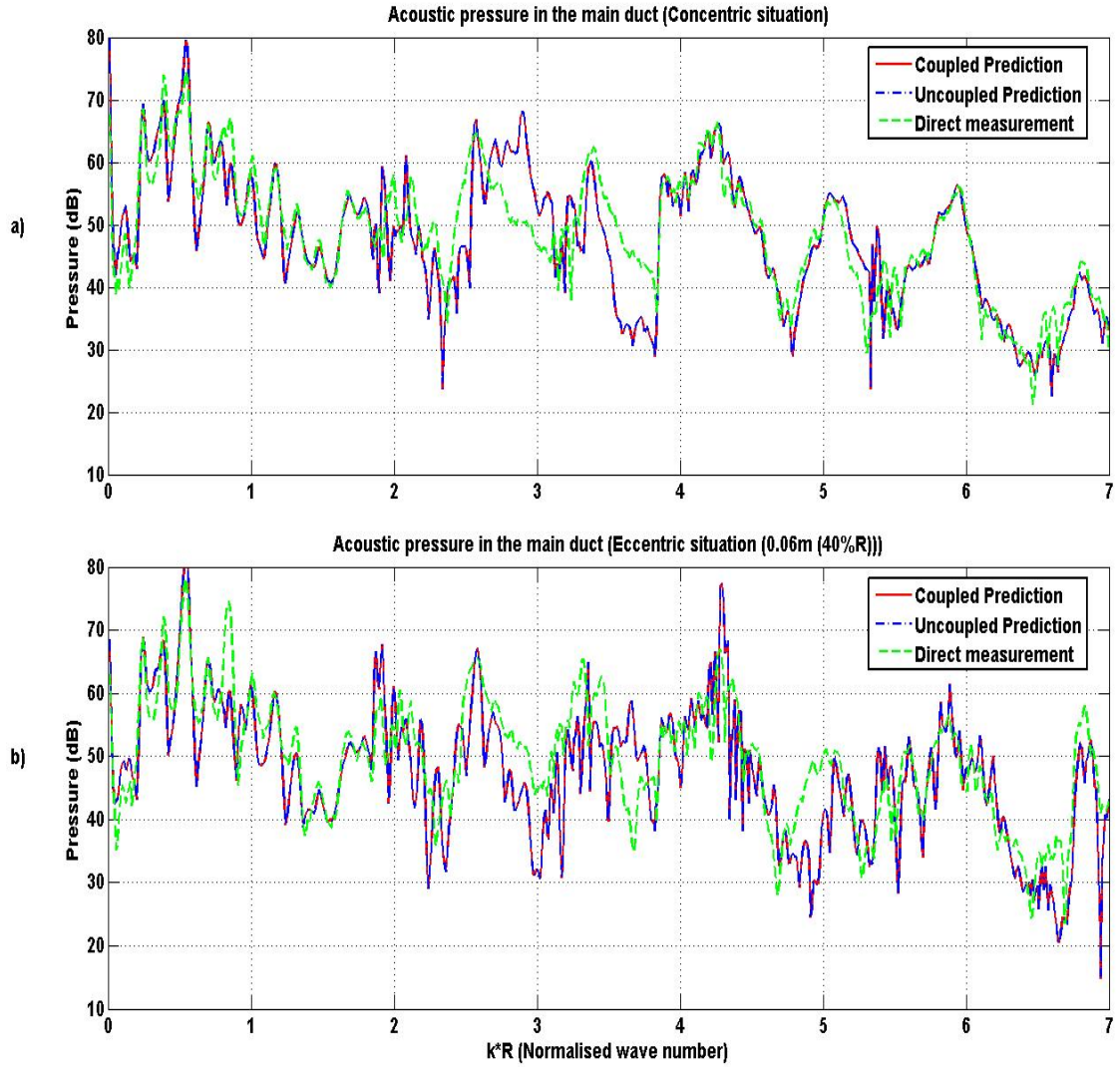

Fig. 4. Comparison between the coupled predictions and the direct measurements for point source excitation: *a*) source concentric ($\delta = 0m$); *b*) source eccentric ($\delta = 0.06m(40\%R)$).

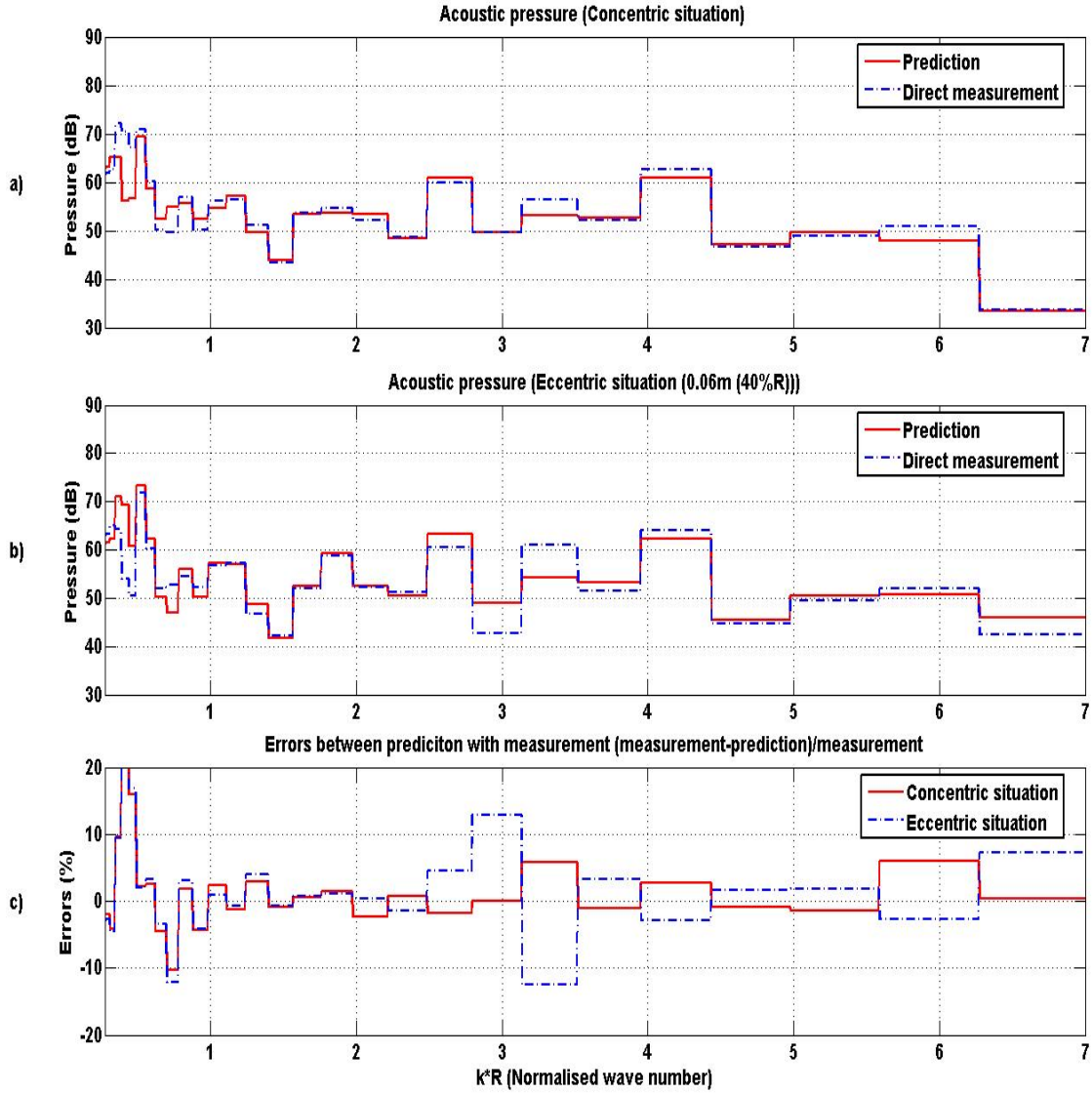

Fig. 5. Comparison between the coupled predictions and the direct measurements for point source excitation: *a*) source concentric ($\delta = 0m$); *b*) source eccentric ($\delta = 0.06m(40\%R)$)); *c*) percentage errors.

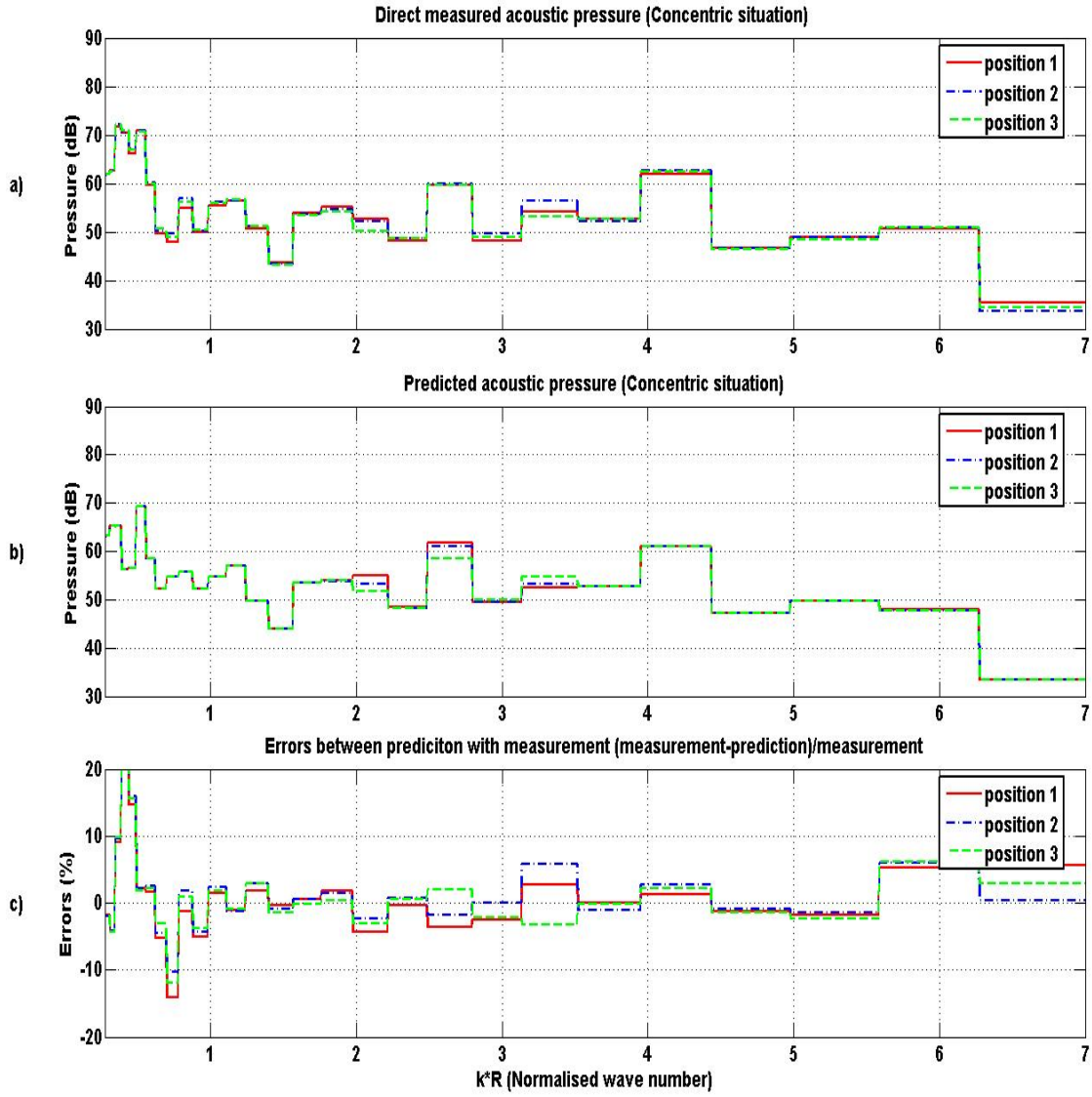

Fig. 6. Comparison of the errors around the circumference of the main duct for a concentric point source: *a*) direct measurements; *b*) predicted results; *c*) percentage errors.

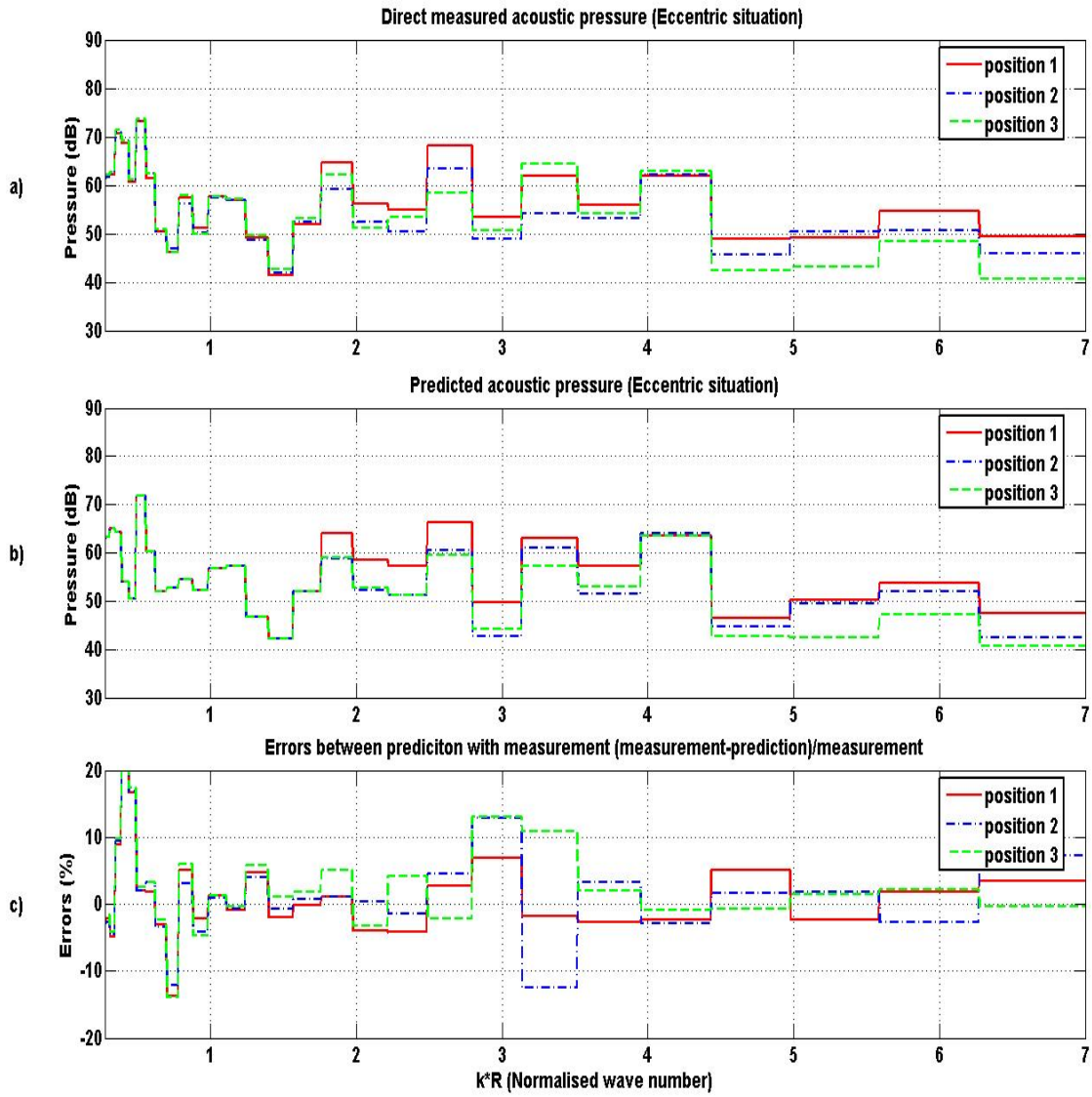

Fig. 7. Comparison of the errors around the circumference of the main duct for an eccentric point source: *a*) direct measurements; *b*) predicted results; *c*) percentage errors.

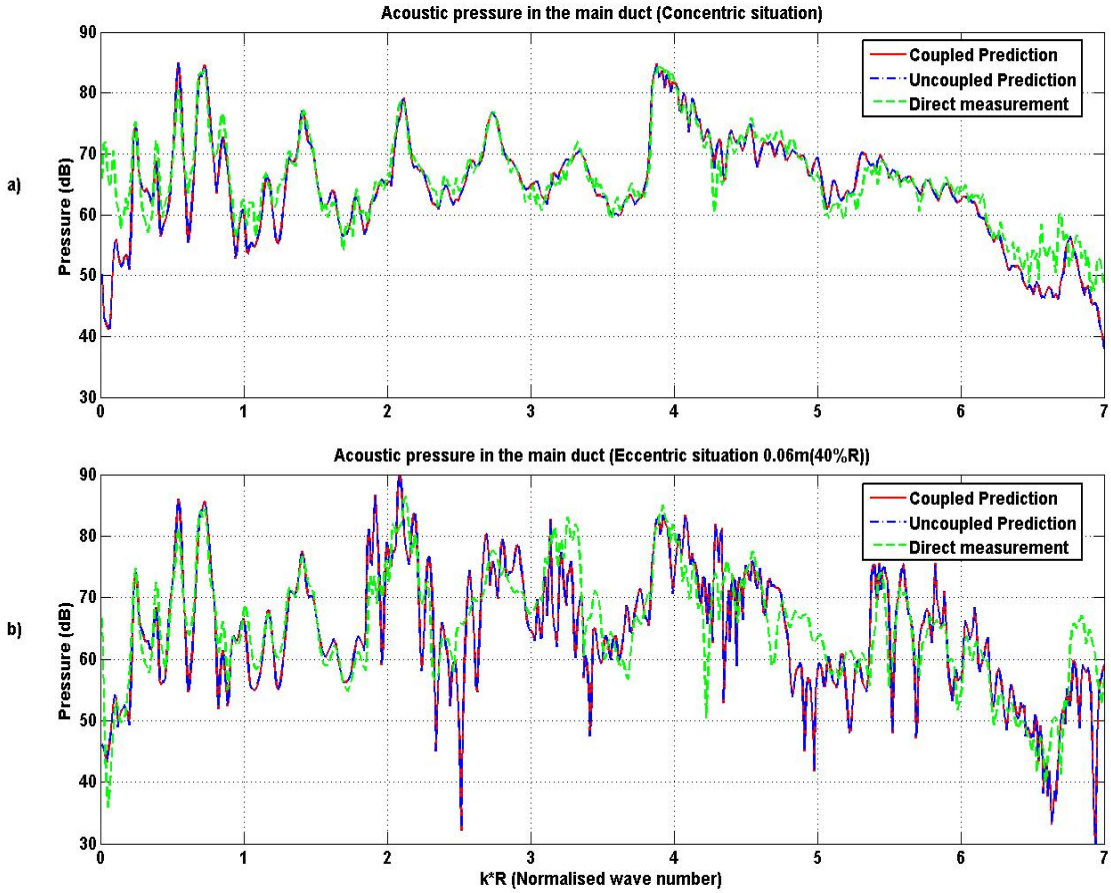

Fig. 8. Comparison of the coupled and uncoupled predictions with direct measurements for the plane wave source: *a*) source concentric ($\delta = 0m$); *b*) source eccentric ($\delta = 0.06m(40\%R)$)).

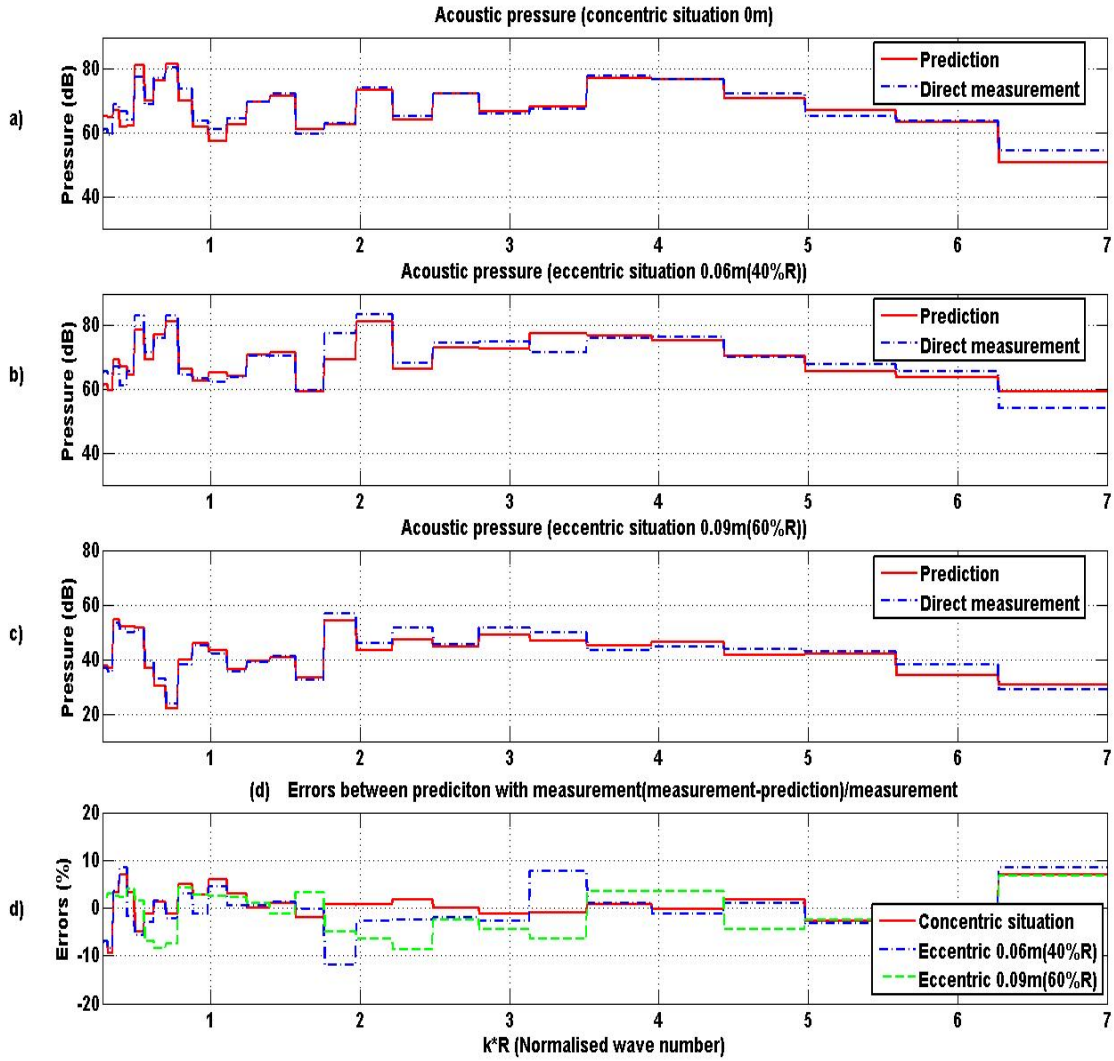

Fig. 9. Comparison of the errors for the concentric and eccentric plane wave source: *a*) source concentric; *b*) source eccentric $\delta = 0.06m(40\%R_0)$; *c*) source eccentric $\delta = 0.09m(60\%R_0)$; *d*) percentage errors

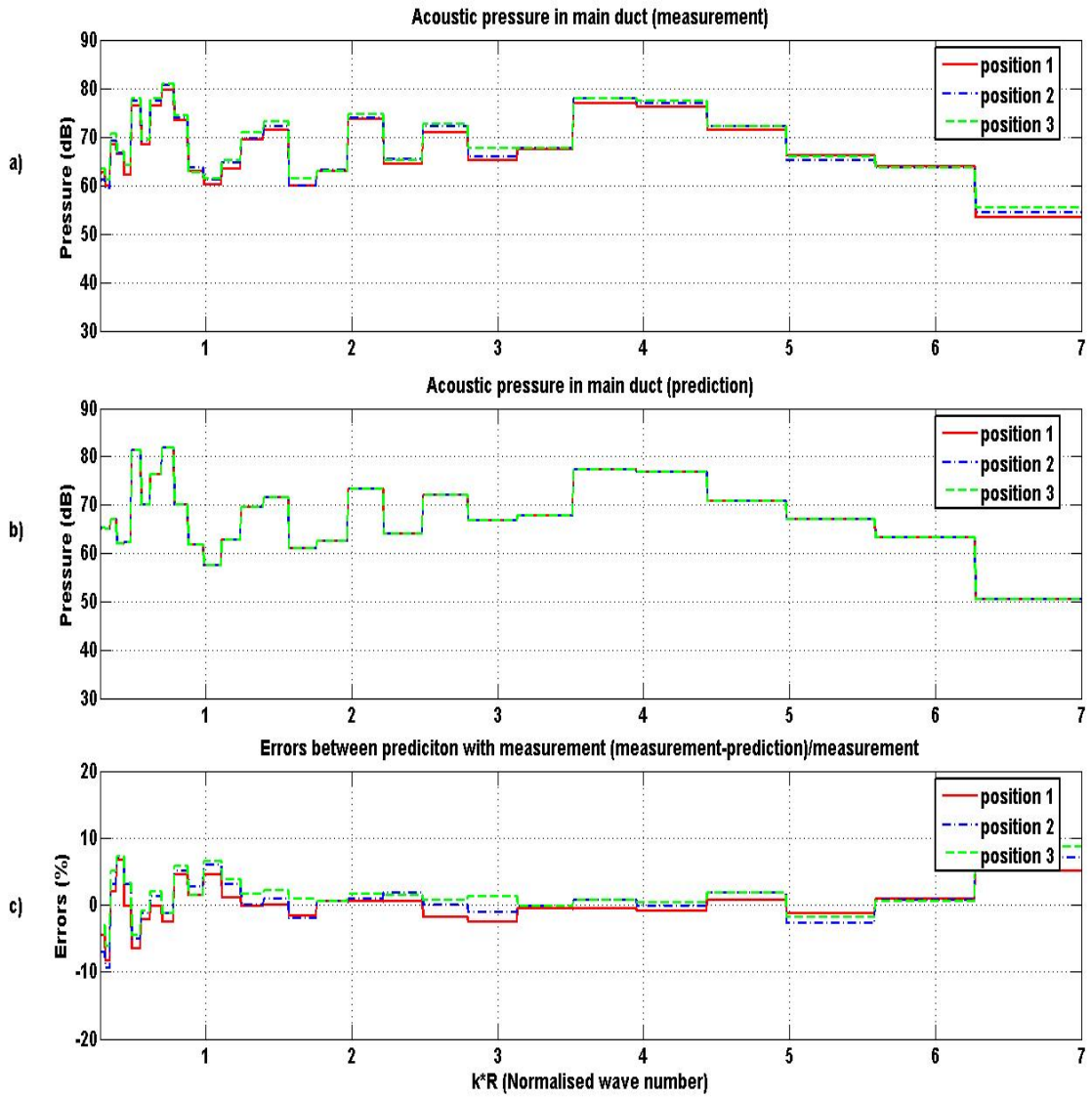

Fig. 10. Comparison of the errors around the circumference of the main duct for a concentric plane wave source: *a*) direct measurements; *b*) predicted results; *c*) percentage errors.

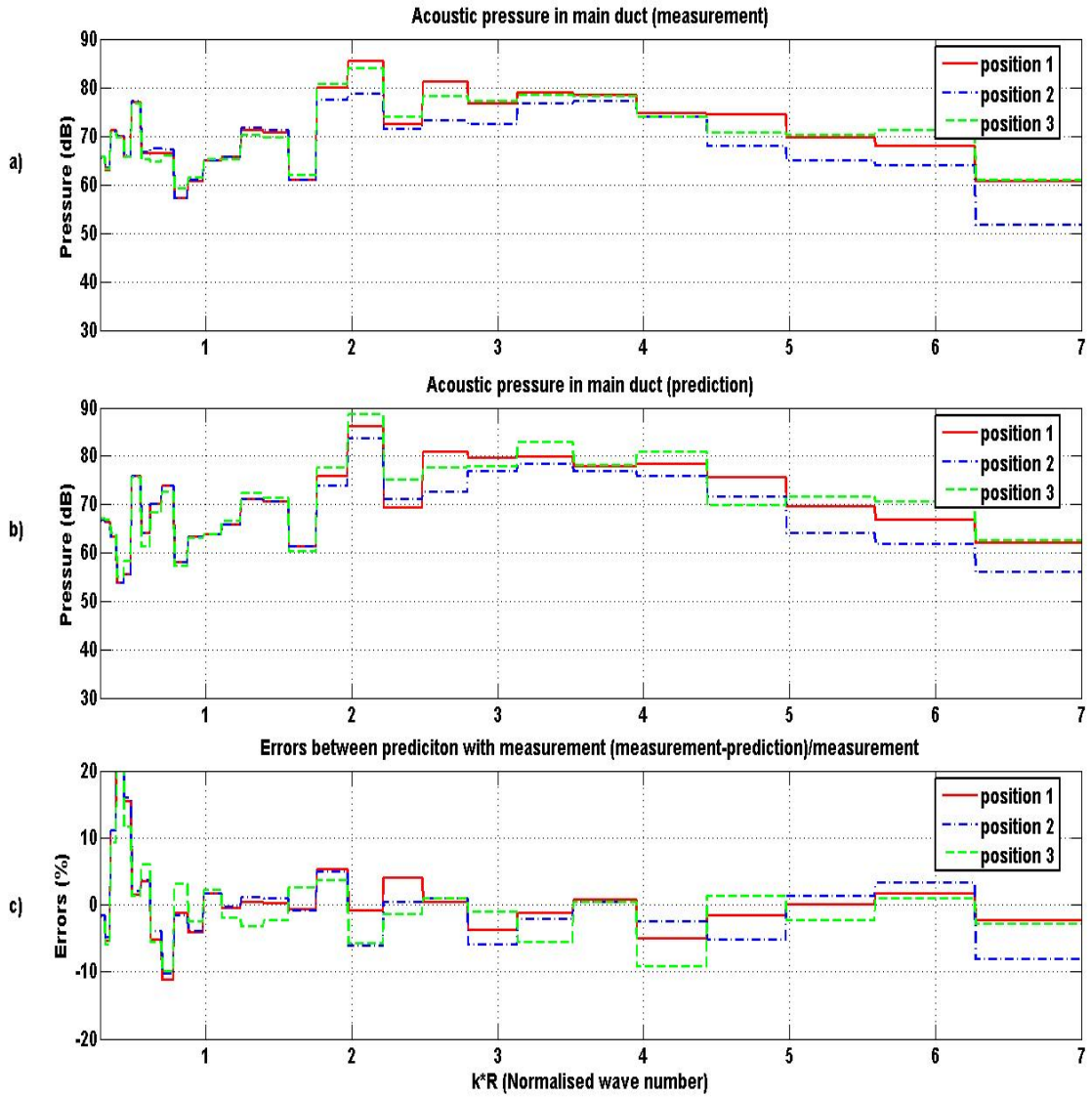

Fig. 11. Comparison of the errors around the circumference of the main duct for an eccentric plane wave source: *a*) direct measurements; *b*) predicted results; *c*) percentage errors.